Solar Thermal Processing to Disinfect Human Waste – Supplementary Materials

Richard P. Fisher[1], Allan Lewandowski[2], Tesfayohanes W. Yacob[3], Barbara J. Ward[3], Lauren M. Hafford[3], Ryan B. Mahoney[3], Cori J. Oversby[3], Dragan Mejic[1], Dana H. Hauschulz[1], R. Scott Summers[3], Karl G. Linden[3], Alan W. Weimer[1*]*

AUTHOR ADDRESS

[1] University of Colorado at Boulder, Department of Chemical and Biological Engineering, 3415 Colorado Ave, UCB 596, Boulder, CO 80309-0596;

[2] Solar Consulting, LLC, 505 Madison Street, Denver, CO 80206

[3] University of Colorado at Boulder, Department of Civil, Environmental, and Architectural Engineering, 4001 Discovery Drive, UCB 607, Boulder, CO 80309-0607

Corresponding Authors: Alan W. Weimer (alan.weimer@colorado.edu) and Karl G. Linden (karl.linden@colorado.edu)

KEYWORDS

Keywords: Finite element, heat transfer, kinetics, pyrolysis, solar flux image

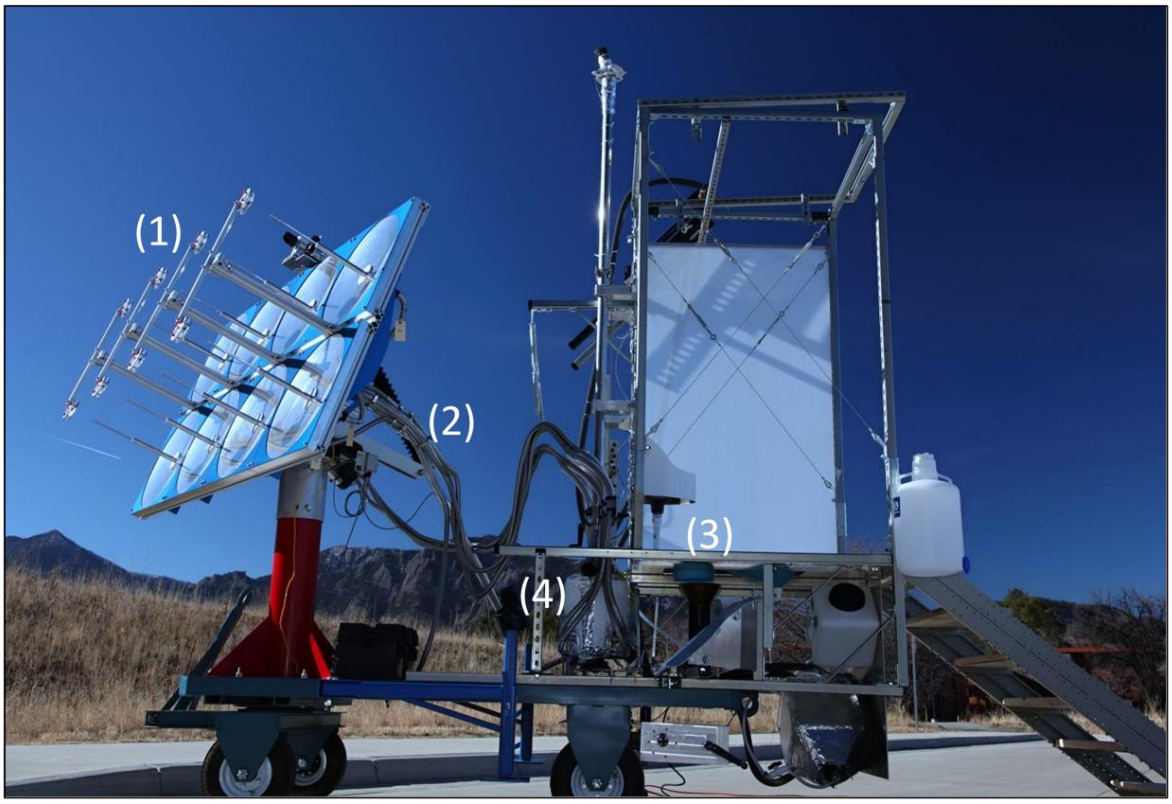

Figure S1. The Sol-Char Sanitation Prototype. Noted in the photograph are the (1) parabolic concentrators, (2) fiber optic bundles, (3) the squat plate toilet, and the (4) solarthermal reactor.

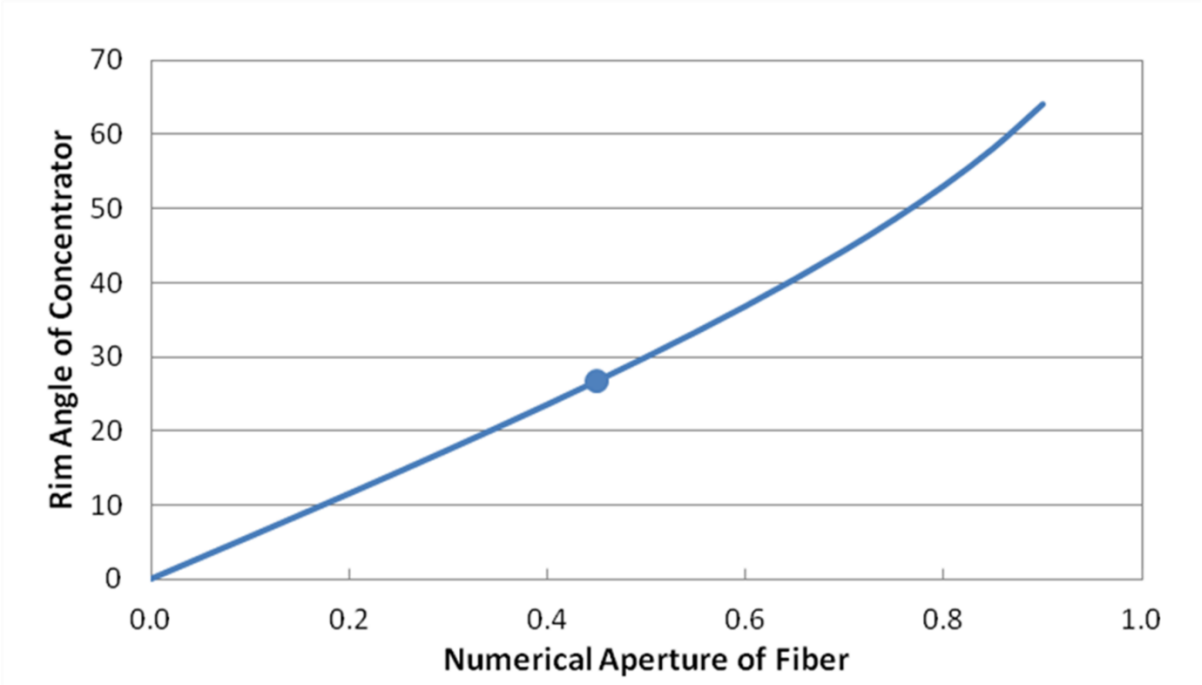

Figure S2. Concentrator-fiber relationship. The data point represents the design point chosen for the system.

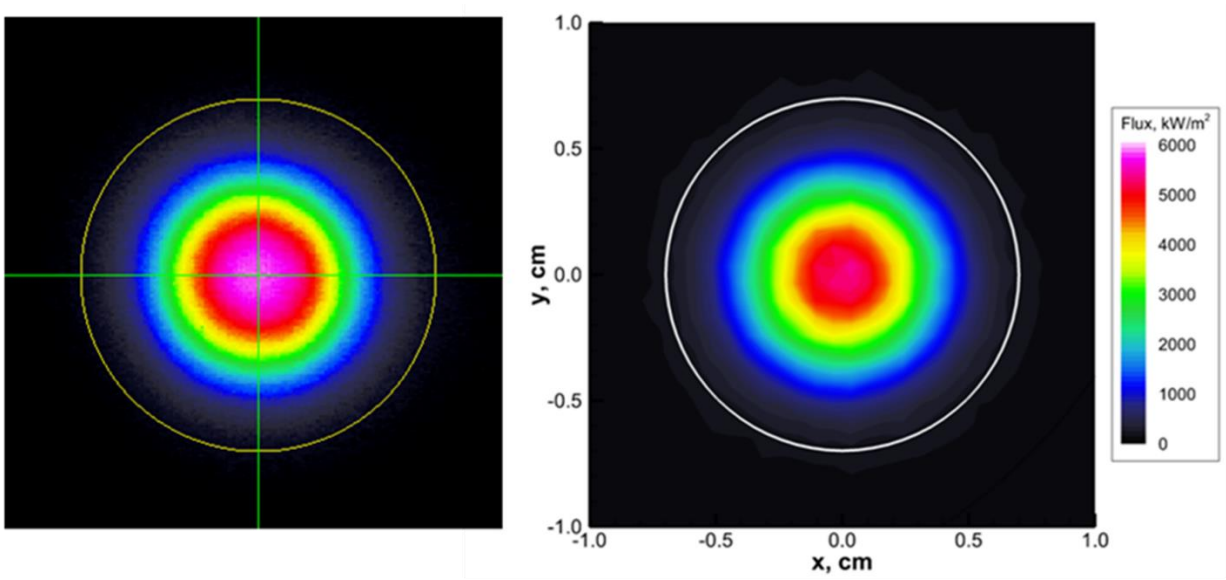

Figure S3. Measured flux map at the redirected focal point (left). The predicted flux map (right) is shown at the same linear scale and same relative color scale. The measured flux map has not been scaled to intensity.

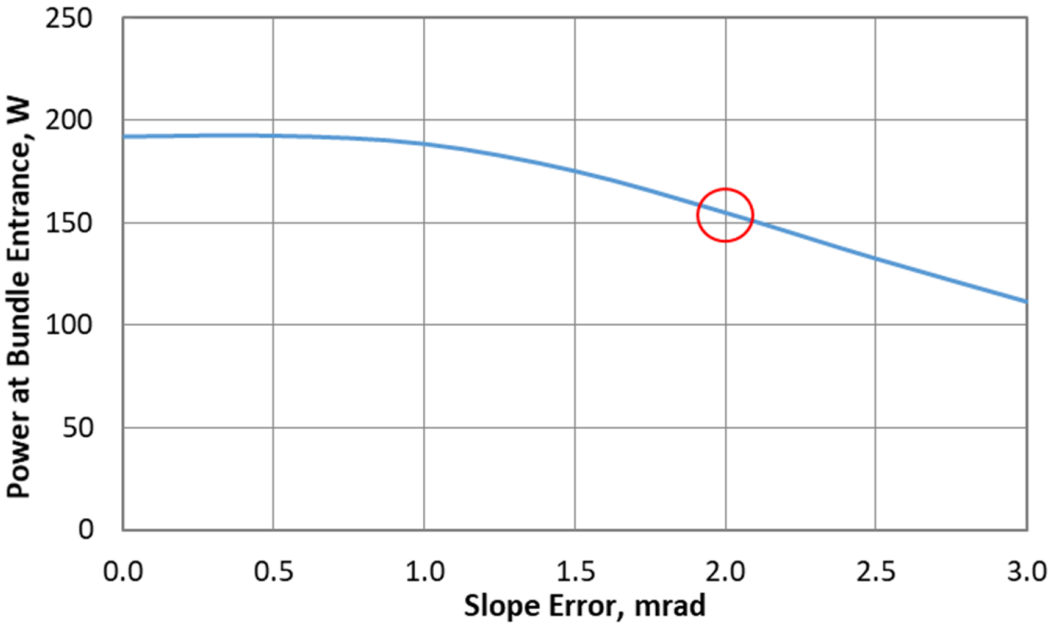

Figure S4. Impact of concentrator slope error on power available at the 12.5mm diameter aperture of the fiber optic bundles. The red circle shows the approximate value of slope error matching the average delivered power of the eight concentrators.

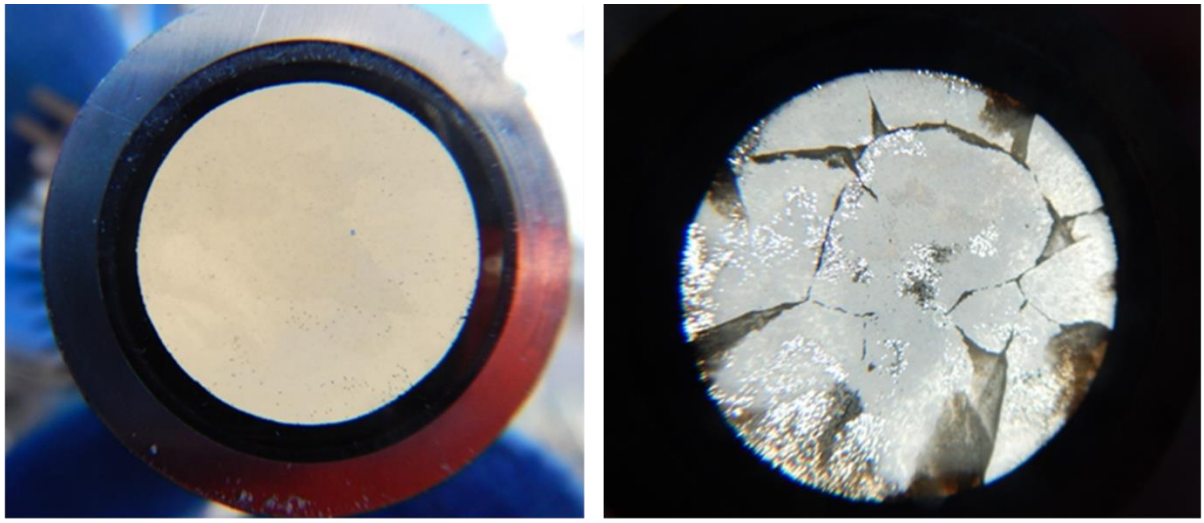

Figure S5. Acrolite bundle A4 (A end) showing 12.5mm fused bundle and housing in the ferrule before on-sun testing (left). The area between the bundle and ferrule is black glass. There are an unavoidable number of broken fibers which can be seen as small black spots within the bundle. For comparison A4 (B end) is shown after on-sun receiver testing.

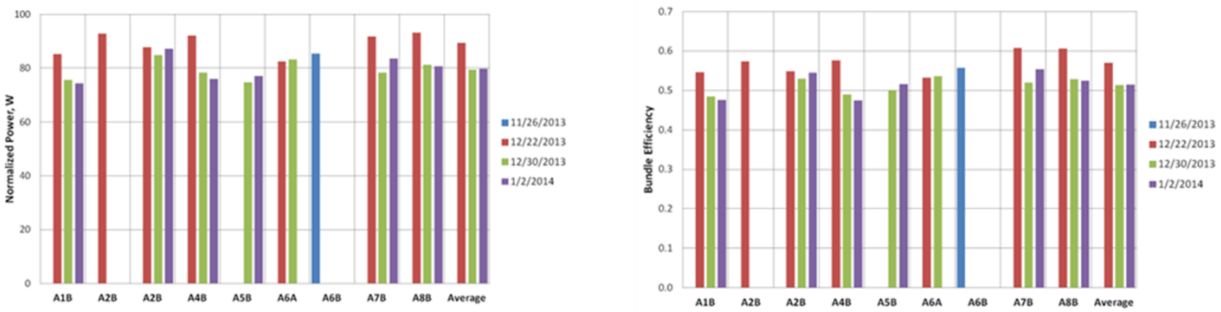

Figure S6. Bundle performance showing normalized power (left) and efficiency or net transmittance (right).

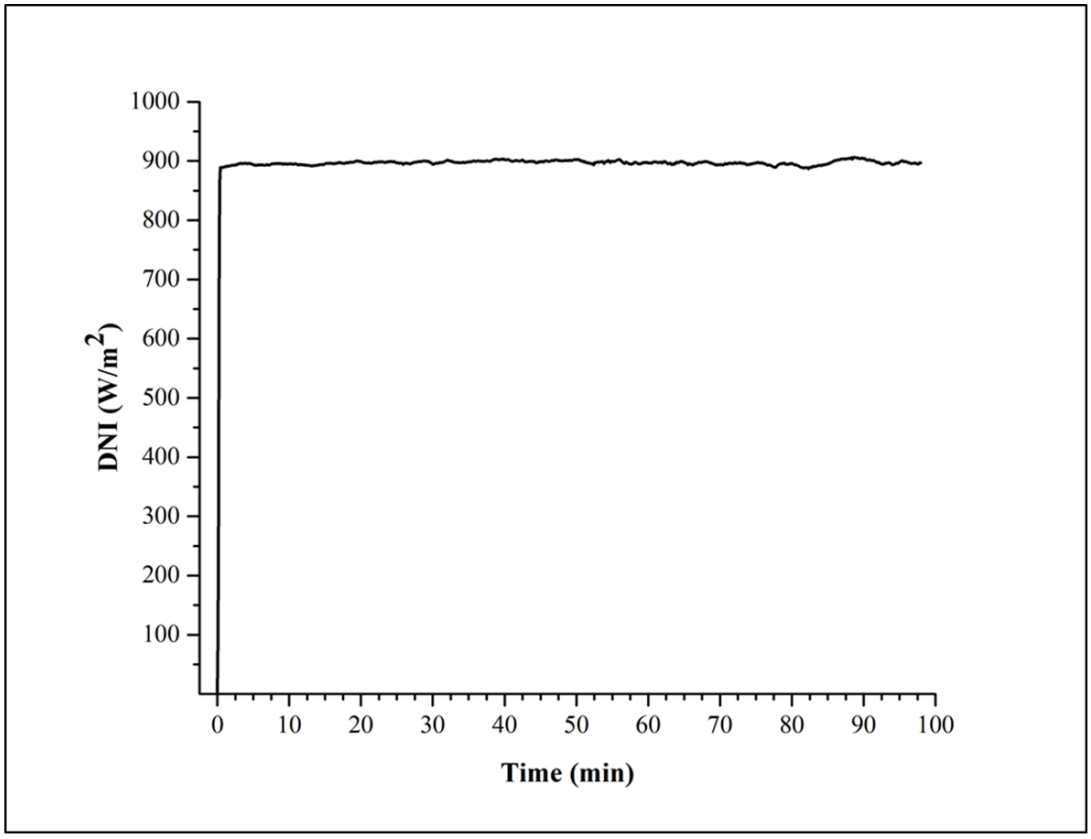

Figure S7. Experimental data from July 3, 2014, showing the Direct Normal Irradiance (W/m^2) over the experimental period.

Table S1. Initial values selected for solar concentrator sizing.		
Component	**Chosen Value**	**Comment**
Primary reflectivity	0.85	Depends on material
Turning mirror reflectivity	0.95	Typical silvered thin glass value
Intercept at homogenizing rod	0.9	Depends on accuracy and fiber diameter
Homogenizing rod Fresnel reflection	0.965	Fresnel reflection for n=1.46
Homogenizing rod transmittance	1.0	Should be high value for quartz
Homogenizing rod Fresnel reflection	0.965	Fresnel reflection for n=1.46
Fiber Fresnel reflection	0.965	Fresnel reflection for n=1.46
Fiber fill factor	0.85	Loss for packing of small diameter fibers
Fiber transmission	0.8	Depends on type of fiber selected and length
Fiber Fresnel reflection	0.965	Fresnel reflection for n=1.46
Overall Efficiency	**0.43**	

Table S2. Optical and geometric inputs for concentrator analysis.	
Sunshape	CSR10 (Neumann 2002)
Direct Irradiance	1000W/m^2
Concentrator Diameter	0.60m
Concentrator Area	0.283m^2
Focal Length	0.69m
Curvature	Parabolic
Contour Slope Errors*	1.0mrad
Contour Specularity Errors*	0.5mrad
Mirror Reflectivity	0.95
Support Arm Width	2.54cm
Turning Mirror Diameter	11.5cm
Curvature	Flat
Mirror Slope Errors*	0.5mrad
Mirror Specularity Errors*	0.1mrad
Turning Mirror Reflectivity	0.95
Turning Mirror Position	0.85f
Homogenizing Rod Diameter	13.5mm
Homogenizing Rod Length	61cm
Homogenizing Rod Index	1.46
Rod Slope Errors*	0.2mrad
Rod Specularity Errors*	0.05
Rod Entrance Position	0.7f

*Standard deviation of normally distributed error

Model Development

Researchers from the University of Colorado at Boulder have designed, built and demonstrated a novel prototype process for disinfecting and potentially pyrolyzing human fecal waste using concentrated solar power. During the course of the project, the authors developed a simple and preliminary COMSOL® multiphysics pyrolysis model as a process design tool for batch disinfection and possible pyrolysis of human feces. The model encompasses many of the key physics in the disinfection and pyrolysis process: concentrating solar power, variable solar conditions, and reaction kinetics to predict conversion. Several inputs to the model were derived from experiment and literature. The model is fit to experimental results by adjusting the effective thermal conductivity of the feces during prototype testing. The key result from the modeling is an expression for the effective thermal conductivity of untreated human feces, and other wet-solid materials, that accounts for "wet" and "dry" stages and that can be incorporated into any heat transfer model.

Geometrical Considerations

The feces contained in the Sol-Char reactor was modeled as a solid cylinder cut into a one-quarter symmetrical section, shown in Figure SI-8, built and simulated using COMSOL™ Multiphysics finite element software.

The physical dimensions of the reactor are shown in Table SI-3 and were used in the simulation. Since the thickness of the stainless steel reactor wall is more than an order of magnitude smaller than the thickness of the feces domain, and, the thermal conductivity of steel is more than an order of magnitude greater than that of feces, the steel wall was not modeled explicitly due to its negative impact on the mesh quality. Instead the steel wall was treated with a

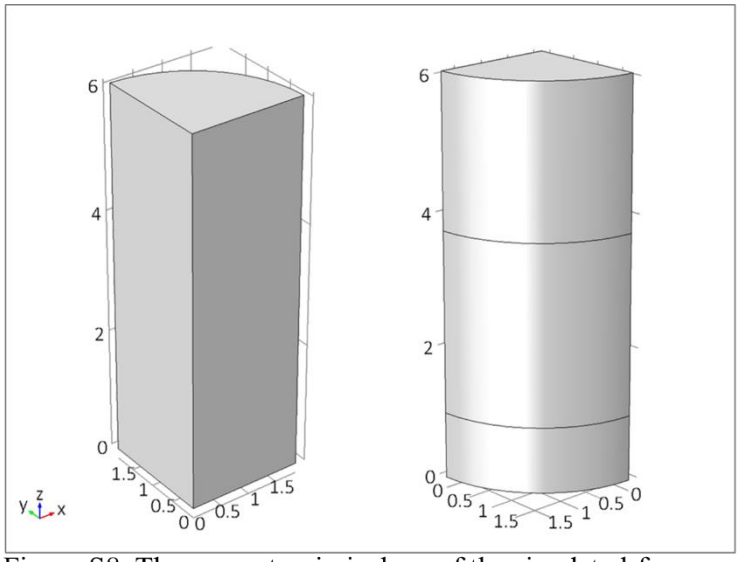

Figure S8. The geometry, in inches, of the simulated feces in COMSOL (R) Multiphysics. The dimensions are listed in Table S-3.

Very Thin Conductive Layer (VTCL) boundary condition rather than a meshed domain. The outer surface of the reactor was also painted with flat black solar absorbing paint, Tempil® Pyromark® 2500, which has high absorbance for solar spectrum wavelengths.

Model

Temperature fields in the feces domain were modeled by a transient conduction model with isotropic temperature-dependent physical properties approximated by analytic functions for thermal conductivity ($\boldsymbol{k}$), heat capacity ($\boldsymbol{C_p}$), and density ($\boldsymbol{\rho}$), with nominal

Table S3. Geometrical dimensions of the Sol-Char Sanitation prototype.

Dimension	Value	Description
R	0.047752 [m]	ID of reaction vessel
L	0.003048 [m]	Thickness of vessel wall
H	0.15403 [m]	Height of feces studied in experiment

values listed in Table S-4.

$$\rho C_P \frac{\partial T}{\partial t} + \rho C_p \vec{\boldsymbol{u}} \cdot \nabla T = \nabla \cdot (k \nabla T) + Q \quad (1)$$

where Q is a heat source applied to the waste boundary by the solar flux.

Table S4. Thermophysical properties used in the simulation.

Variable	Value	Description
ρ_{F0}	1450 [kg/m^3]	Initial density of feces at ambient temperature
ρ_C	500 [kg/m^3]	Density of char produced from feces pyrolysis
k_{F0}	0.39 [W/m-K]	Thermal conductivity of pit latrine waste in Durban, SA
k_C	0.19 [W/m-K]	Thermal conductivity of char
$C_{p,F0}$	2200 [kJ/kg-K]	Heat capacity of pit latrine waste in Durban, SA
T_{amb}	20 [°C]	Ambient temperature in experiment and simulation
T_{vap}	94 [°C]	Boiling point of water in Boulder, CO (experiment site)
T_{rxn}	250 [°C]	Pyrolysis reaction initiation temperature
ε	0.88	Emissivity of Pyromark® 2500 solar paint
σ	5.67x10^{-8} [W/m^2-K]	Stefan-Boltzman constant for radiative heat flux
a	0.95	Absorbance of Pyromark® 2500 solar paint
Q_{fiber}	78.1 [W]	Average normalized power from one optical fiber

Extent of conversion was also modeled in the simulations by a Distributed Activation Energy Model (DAEM) following the methods of Miura and Maki [1, 2]. The kinetic expression for conversion follows the form

$$\frac{d\alpha}{dt} = A_\alpha \exp\left(-\frac{E_\alpha}{RT}\right)(1-\alpha), \qquad \alpha(0) = 0 \tag{2}$$

where A_α is the pre-exponential factor, E_α is the activation energy for a given value of the extent of conversion, α, between 0 and 1. In the DAEM proposed by Miura and Maki, A_α and the E_α can vary with extent of conversion. The variations of A_α and E_α determined for the present study are shown in Figure SI-9. Since the Miura-Maki method doesn't determine a single value for either $A_\alpha$or E_α, an interpolation between the points was performed in COMSOL™ in order to obtain a solution to the coupled systems of equations for heat transfer and reaction kinetics.

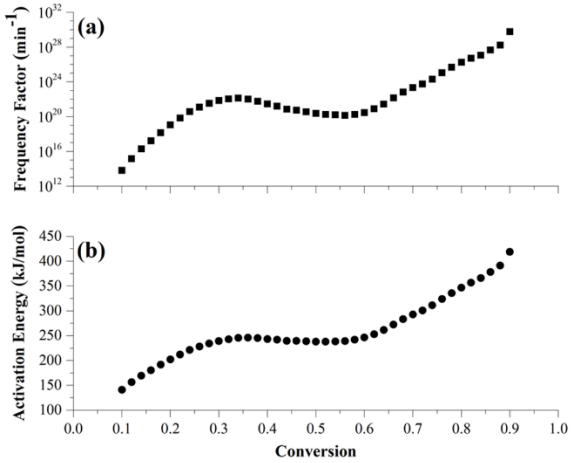

Figure S9. Variation of the kinetic parameters derived from the DAEM, (a) frequency factor, A_α, and (b) activation energy, E_α, with extent of conversion, α

Since the Sol-Char sanitation receiver is a batch reactor, $\vec{\boldsymbol{u}} = 0$ so that equation 1 becomes

$$\rho_F C_{p,F} \frac{\partial T}{\partial t} = \nabla \cdot (k_F \nabla T) + Q \tag{3}$$

The subscript F denotes the property for feces (reactants), subscript C denotes the property value for char (products), and the naught subscript denotes the initial value of a property. Physical properties ρ_F, k_F, and $C_{p,F}$, were assumed to be constant with respect to temperature until either the vaporization temperature of water or pyrolysis reaction temperature, denoted as T_{vap} and T_{rxn}, respectively, was reached. The smoothed step change from one value to another is

approximated by the smoothed Heaviside function, $U(x)$, which can be expressed as the integral of the Dirac delta function, $\delta(s)$, at a given point x

$$U(x) = \int_{-\infty}^{x} \delta(s)ds \tag{4}$$

Density of the feces, ρ_F, was approximated as a smoothed step change from the nominal value, ρ_{F0}, to that of typical biomass char, ρ_C, as extent of conversion, α, varies from 0 and 1.

$$\rho_F(T) = \rho_{F0} - (\rho_{F0} - \rho_C)U(\alpha) \tag{5}$$

Heat capacity of the feces, $C_{p,F}$, was also approximated with a similar expression that incorporates the latent heat of vaporization and endothermic heat of reaction for biomass pyrolysis, shown in Figure S10,

$$C_{p,F}(T) = C_{p,F0} + \Delta\left[\frac{\lambda_{vap}}{\Delta T}U(T_{vap})\right] + \Delta\left[\frac{H_{rxn}}{\Delta T}U(T_{rxn})\right] \tag{6}$$

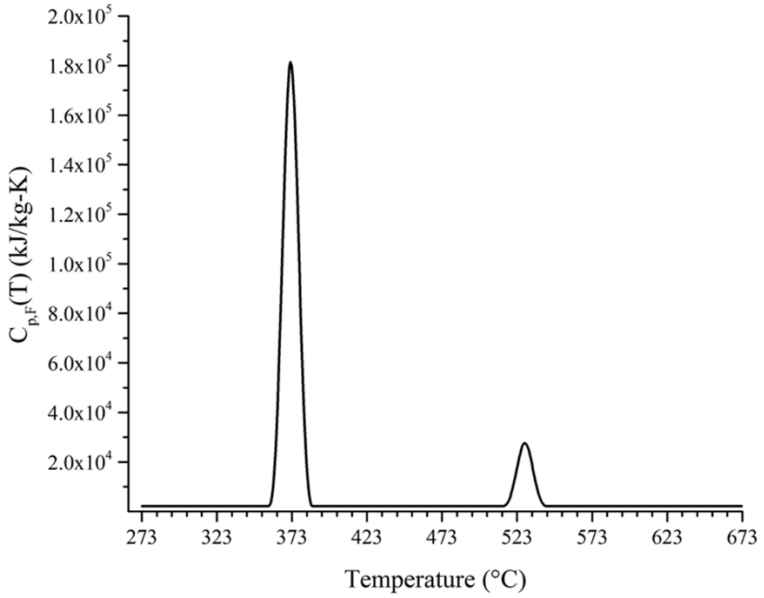

Figure S10. Function used in COMSOL to describe the heat capacity of waste over a temperature range that includes vaporization and pyrolysis. The area under the curve is equal to that of the sum of latent heat of vaporization and endothermic heat of pyrolysis.

where the shorthand expressions

$$\Delta\left[\frac{\lambda_{vap}}{\Delta T}U(T_{vap})\right] = \frac{\lambda_{vap}}{\Delta T}U(T_{vap}) - \frac{\lambda_{vap}}{\Delta T}U(T_{bp}+\Delta T) \quad (7)$$

$$\Delta\left[\frac{H_{rxn}}{\Delta T}U(T_{rxn})\right] = \frac{H_{rxn}}{\Delta T}U(T_{rxn}) - \frac{H_{rxn}}{\Delta T}U(T_{rxn}+\Delta T) \quad (8)$$

denote a "step up" and a "step down" from the nominal value of heat capacity, $C_{p.F0}$, which accounts for the energy required to evaporate water and then pyrolyze the feces to char over a very small temperature change ΔT. The area under the curve in Figure S10 is equal to that of the latent heat of vaporization of water, $\lambda_{vap} = 2260$ kJ/kg, and endothermic heat of biomass pyrolysis found by Van de Velden, et al., to vary between 207 and 434 kJ/kg [3]. The simulation results were found to be insensitive to the value of the endothermic heat of biomass over the range of values presented by Van de Velden, et al.

Effective thermal conductivity of feces, k_F, was approximated by a similar expression

$$k_F(T) = \beta_F\big(k_{F0} - [k_{F0} - k_C]U(\alpha)\big) \quad (9)$$

where β_F is a coefficient used to adjust the thermal conductivity of feces. The expression for β_F is dependent upon temperature T

$$\beta_F = \beta_{wet} - \big(\beta_{wet} - \beta_{dry}\big)U\big(T_{vap}\big) \quad (10)$$

When the waste reaches the temperature T_{vap}, the coefficient β_F undergoes a step change from β_{wet} to β_{dry} as the feces are first dried out and then further heated to pyrolysis temperatures. The coefficient β_F accounts for the presence of water in untreated human feces, as well as for the

unmeasurable effects in the experimental system, e.g. partial oxidation of the feces that promotes heat transfer.

A boundary heat source, Q, from the concentrated solar power illuminating the reactor (Figure S11), was applied to the feces outer boundary, shown by Figure S12. Flux map

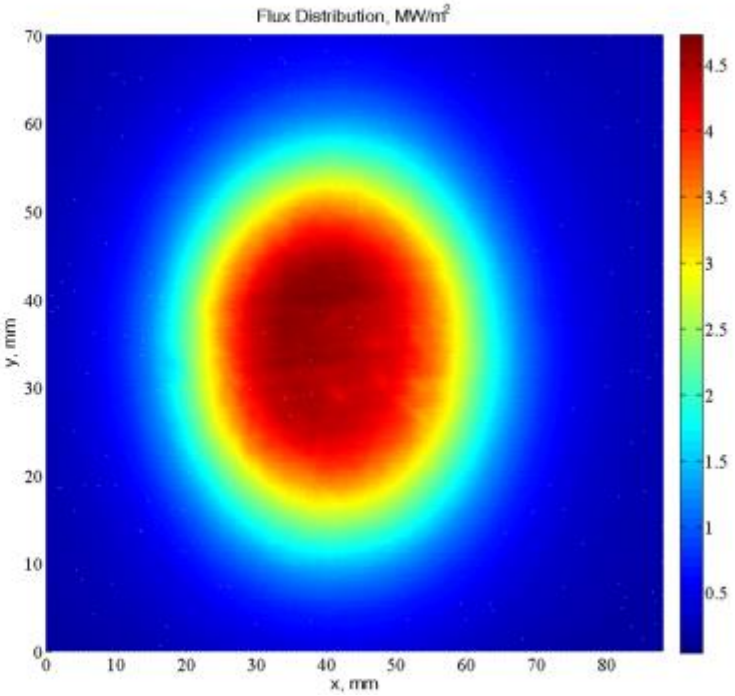

Figure S11. Normalized flux distribution from images obtained for the Sol-Char Sanitation prototype. The optical fiber was situated in front of an opaque quartz plate and a camera behind the plate was used to capture the image. The normalized power exiting the fiber was measured to be 78.1 W. The direct normal irradiance was also measured during the image capture with a Kipp & Zonen CHP-1 normal incidence pyrheliometer.

images can be imported directly into COMSOL® and are used as a scaling function on the total power applied to the geometry. The solar flux is absorbed by the painted outer surface of the reaction vessel, shown as

$$Q = aQ_{fiber}k_{image} \tag{11}$$

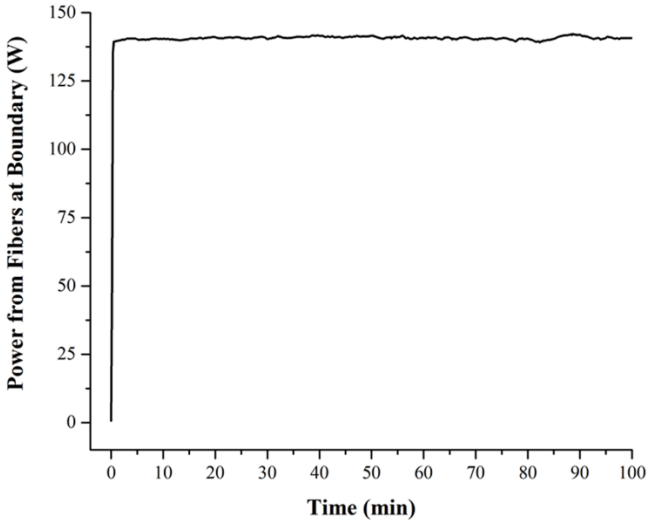

Figure S12. Integrated heat flux on waste boundary from two optical fibers on the Sol-Char Sanitation prototype. This value matches the power measured in experiment by a Coherent PM-150 UCB power meter.

where a is the surface absorbance of Tempil® Pyromark® paint, Q_{fiber} is the normalized power output of one optical fiber, and k_{image} is an expression that incorporates the pixelated values from the flux map images, $f(r\theta, z)$, and a scale factor to ensure that the integral of the flux across the boundary equals the observed power during experiment

$$k_{image} = 3.13 f(r\theta, z) \tag{12}$$

where $r\theta$ is the arclength along the boundary surface and z is the vertical position on the boundary, associated with the location and the saturation value $0 \leq f(r\theta, z) \leq 1$ in the flux map image.

A VTCL boundary condition is used on these boundaries, allowing the thermal conductivity effects of the steel reactor wall to be simulated without the need to mesh another solid domain in the model. The VTCL boundary condition computes the temperature flux across a layer of a given thickness, L

$$-\hat{\boldsymbol{n}} \cdot (-k\nabla T) = L\left(Q - \rho_L C_{p,L}\frac{\partial T}{\partial t}\right) - \nabla_L \cdot (-Lk_L \nabla_L T) \quad (13)$$

The thermophysical properties, k_L, ρ_L, and $C_{p,L}$, of the wall were set to the value of type 316 stainless steel, shown in Table S4, and L is the thickness of the reaction vessel wall.

Radiation (emission) was included as another boundary condition in the same locations as the heat source, Q, since these boundaries are not insulated from ambient. This boundary condition accounts for heat lost to the ambient environment as the temperature of the reactor surface increases

$$-\hat{\boldsymbol{n}} \cdot (-k\nabla T) = \varepsilon\sigma(T_{amb}^4 - T^4) \quad (14)$$

where σ is the Stefan-Boltzman constant, ε is the surface emissivity of the painted steel reactor, and T_{amb} is the ambient air temperature. These values are also shown in Table S4.

Results

The model developed in this work was ultimately compared to data collected for the Sol-Char Sanitation prototype on July 3, 2014. This day was especially sunny, with direct normal irradiance (DNI) measured at average 900 W/m^2 for several hours, as can be seen in Figure 7. The average power measured from each fiber optic bundle was found to be 78.1 W, after being normalized to a standard DNI of 1000 W/m^2. Feces from four healthy adults were collected in the reactor prior to the experiment, weighing approximately 800 g total. The volume of the charge to the reactor was approximately 600 cm^3.

conductivity as defined by equations 9 and 10, were optimized to fit the experimental data obtained during solarthermal drying on July 3, 2014, using least squares minimization. The coefficients β_{wet} and β_{dry} were the optimization parameters adjusted to evaluate the sum squared error (SSE) between experimental temperatures and the simulated temperatures, predicted by the model, until the SSE was minimized. The final values of the coefficients of the effective thermal conductivity, β_{wet} and β_{dry}, are listed in Table 1. The response of the effective thermal conductivity, $k_F(T)$, to both temperature and extent of conversion is shown in a contour plot in Figure 9. A comparison of the experimental and simulated temperature data in the Sol-Char Sanitation prototype in Figure 10 shows the close fit of the model predictions to observation.

Conclusions

A simple model for the disinfection of human feces was presented with experimental fitting of feces effective thermal conductivity. This novel expression for the temperature-dependence of thermal conductivity of human feces, or any wet-solid material, is proposed, and can should be improved in future work. Any unknown coefficients or values in the expression can be optimized by a least squares minimization of simulation results based on temperature traces from a representative experimental system, or, a more fundamental expression that includes the placement of feces in the receiver can be developed. The study presented here represents a demonstration of a method for developing and validating empirical models and for simulating complex processes using a simple model. This model and improvements to it have potential utility as design tools for biomass disinfection and pyrolysis processes.

References

1. Miura, K., *A New and Simple Method to Estimate f(E) and k_0(E) in the Distributed Activation Energy Model from Three Sets of Experimental Data.* Energy & Fuels, 1995. **9**: p. 302-307.
2. Miura, K. and T. Maki, *A Simple Method for Estimating f(E) and k_0(E) in the Distributed Activation Energy Model.* Energy & Fuels, 1998. **12**: p. 864-869.
3. Van de Velden, M., et al., *Fundamentals, kinetics and endothermicity of the biomass pyrolysis reaction.* Renewable Energy, 2010. **35**: p. 232-242.